Finger patterns of magnetic flux in bulk $Bi_2Sr_2CaCu_2O_{8+\delta}$ samples

D. Barness,[1] M. Sinvani,[1] A. Shaulov,[1] T. Tamegai,[2] and Y. Yeshurun[1]
[1]*Department of Physics, Institute of Superconductivity, Bar-Ilan University, Ramat-Gan 52900, Israel*
[2]*Department of Applied Physics, The University of Tokyo, Hongo, Bunkyo-ku, Tokyo 113-8656, Japan*
(Received 12 December 2007; revised manuscript received 18 February 2008; published 20 March 2008)

Fingerlike flux patterns, normally observed in superconducting films, are demonstrated in a bulk material. We observed such patterns in $Bi_2Sr_2CaCu_2O_{8+\delta}$ crystals with an artificial barrier separating regions of different magnetic diffusivity, created by irradiating one-half of the crystal with heavy ions. Flux penetration from the nonirradiated part of the crystal, through the barrier, into the irradiated part forms fingerlike patterns in a wide range of temperatures and field ramping rates. The mechanism responsible for the observed patterns is discussed.

DOI: 10.1103/PhysRevB.77.094514 PACS number(s): 74.25.Qt, 74.25.Ha, 74.72.Hs

I. INTRODUCTION

Nonuniform magnetic flux penetration in type II superconductors, creating finger and dendritic patterns, has recently attracted considerable interest.[1–23] Such patterns have been directly observed in a large number of superconducting films employing magneto-optical imaging techniques.[1–14] The existing experimental data, and the recently developed theoretical models,[14–21] suggest that the origin of these patterns is thermomagnetic instability of the vortex matter in the superconducting films.[21–23] The instability arises from local temperature increase due to flux motion, which, in turn, decreases flux pinning and hence facilitates further flux motion. Linear stability analysis,[24] based on the coupled nonlinear Maxwell and thermal diffusion equations, showed that instability in the form of narrow fingers perpendicular to the background electric field occurs when this field exceeds a threshold value E_c.[19] Further analysis, taking into account nonlocal electrodynamics in thin films and the heat transfer to the substrate, showed that E_c is proportional to the film thickness, and that thin films are much more unstable than bulk superconductors, having a stronger tendency for formation of fingering patterns.[25]

In this paper, we show that fingerlike flux patterns can readily be produced also in a bulk material. We have observed nucleation of such patterns in $Bi_2Sr_2CaCu_2O_{8+\delta}$ samples at an artificial barrier formed by irradiating part of the sample with heavy ions. The irradiation process created a sharp border separating two superconducting regions of low and high persistent currents J, giving rise to high and low magnetic diffusivities in the nonirradiated and irradiated parts, respectively. The different diffusivities create a barrier for flux motion through the border between the two parts. A time resolved magneto-optical imaging system was exploited to visually follow the process of finger formation as the flux front hits the barrier created at the interface between the two superconducting regions. This artificial barrier can be controlled by changing temperature, magnetic field, and field ramp rate, thus allowing study of the influence of the barrier height on the finger-shaped flux penetration through the barrier. We notice similarities and differences between the observed patterns in the bulk and those previously obtained in films and discuss the possibility that the two phenomena have a common origin.

II. EXPERIMENT

A series of $2\times1\times0.03$ mm^3 $Bi_2Sr_2CaCu_2O_{8+\delta}$ single crystals ($T_c=92$ K) grown by the floating-zone method[26] was partially irradiated by 5 GeV Pb ions at the Grand Accelerateur National d'Ions Lourds, Caen, with different doses corresponding to matching fields between 5 and 40 G. Using a mask to cover half of the sample, only the uncovered part (1×1 mm^2) was exposed to the irradiation. In this paper, we present typical data for a sample irradiated to a matching field of 40 G, producing columnar defects with an average distance of approximately 0.7 μm. The uniformity of the sample was confirmed by energy dispersive spectroscopy (EDS), using a JEOL 7500 scanning electron microscope.

Magneto-optical images of the induction distribution were taken using an iron-garnet indicator with in-plane anisotropy and a 12 bit Hamamatsu charge coupled device camera with a frame rate ranging between 0.1 and 25 Hz.[27,28] In a typical magneto-optical measurement, the sample was zero-field cooled to a target temperature between 20 and 70 K and was then subjected to external field parallel to the crystallographic c axis of the sample. The applied magnetic field was ramped from 0 up to 200 Oe at different rates between 0.1 and 1000 Oe/s. For a few selected temperatures, the field was ramped up to 1050 Oe at 0.75 Oe/s. Camera integration time used for image acquisition was 20–110 ms. This integration time was always short enough in comparison with the frame sampling rate.

III. RESULTS

We first demonstrate the border created by the irradiation process. Figure 1(a) exhibits a magneto-optical image of the sample taken at $T=24$ K after exposing the sample to an external magnetic field of 400 Oe. The field fully penetrates the sample creating entirely different flux distributions in its two parts, with a sharp border between them. Examination of the image shows a Bean-like flux distribution in the irradiated part [left hand side in Fig. 1(a)] and a distorted[29] dome shape distribution in the nonirradiated part. When the field is raised to 1050 Oe, the two parts of the sample can no longer be distinguished and a Bean-like distribution is observed throughout the whole sample, as shown in Fig. 1(b). The

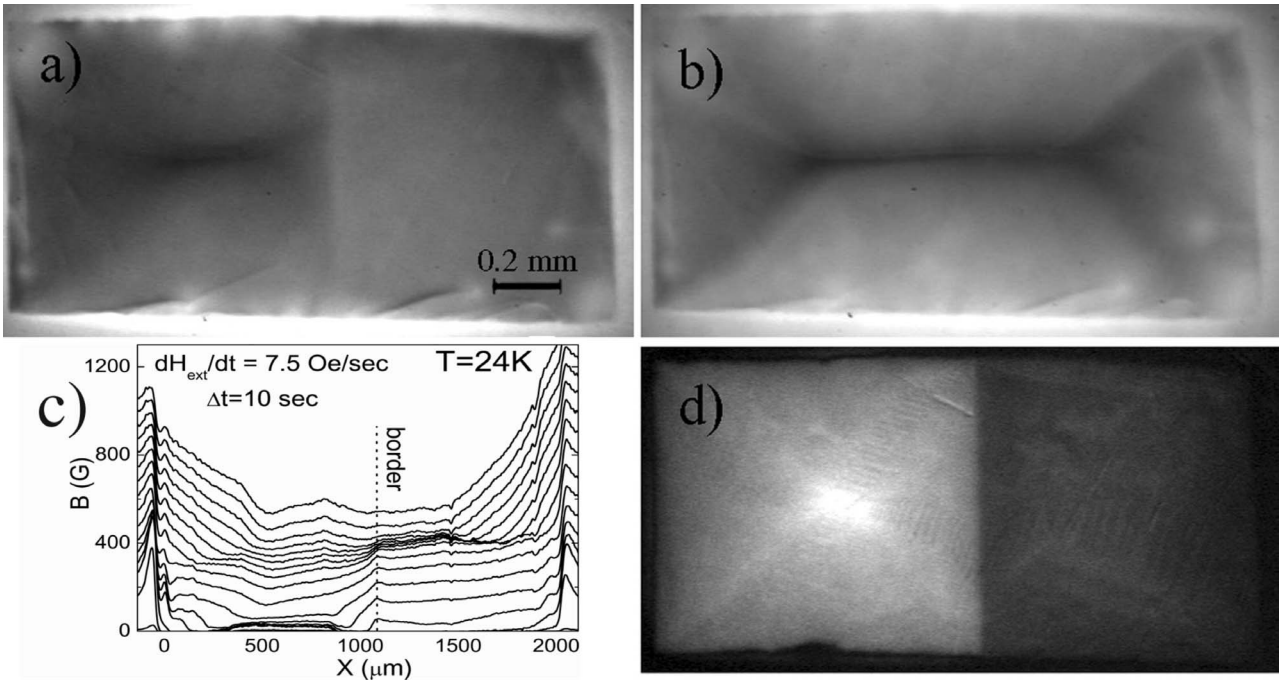

FIG. 1. Magneto-optical images of the partially irradiated sample at 24 K subjected to external field ramped to (a) 400 Oe and (b) 1000 Oe at a rate of 7.5 Oe/s. The left hand side is the irradiated part of the sample. Image contrast was independently rescaled for visual convenience. (c) The whole process can be dynamically viewed by plotting a series of profiles taken across the long side of the sample at the center. (d) After the field is removed, a sharp border between the remnant states of the two parts of the sample is observed.

transition from two distinct induction distributions at low field, to a unified Bean distribution at high field, is also demonstrated in Fig. 1(c). This figure shows the induction profiles measured along a line parallel to the sample long edge and passing through the sample center, while the external field is ramped at a rate of 7.5 Oe/s. For low external fields, the barrier is manifested by a jump in the induction, indicating the presence of screening currents. As the field increases, the screening current at the border decreases until it totally disappears for induction around 400 G, corresponding to the measured order-disorder phase transition induction.[30,31] As the screening current at the border disappears, the induction profiles become Bean-like across the whole sample.[32] We further demonstrate the border between the irradiated and nonirradiated parts by showing the distribution of the remnant induction after reducing the external field back to zero [see Fig. 1(d)]. As expected, flux is mainly trapped in the irradiated part forming the typical Bean roof-top shape.

The field ramping rate has a strong effect on the flux diffusion through the barrier created by the partial irradiation. This is demonstrated in Fig. 2(a) which shows the time dependence of the location x of the flux front moving through the nonirradiated part toward the border and crossing it. The measurements presented in this figure were done

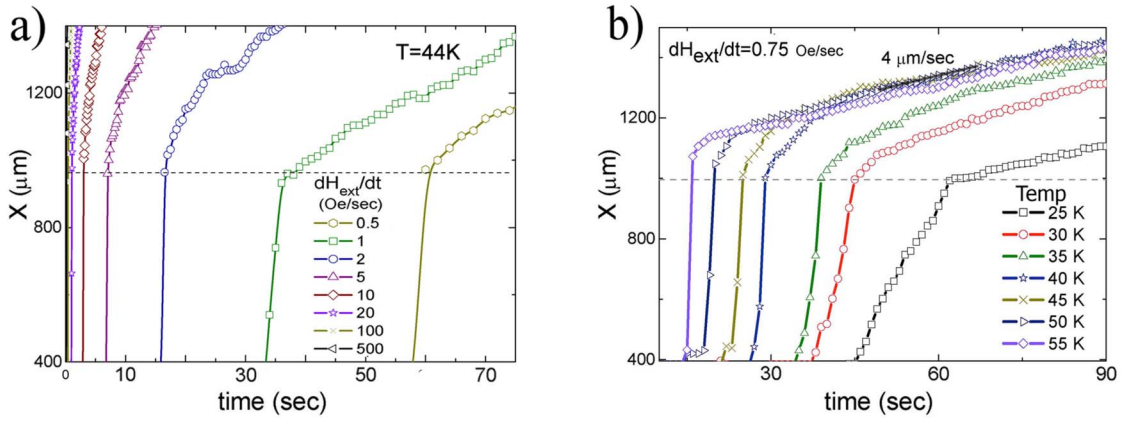

FIG. 2. (Color online) Flux front location as a function of time for (a) various ramping rates (dH_{ext}/dt) ranging from 1 to 500 Oe/s at 44 K and (b) various temperatures between 25 and 55 K at constant ramping rate of 0.75 Oe/s. The irradiation border is marked by a horizontal dashed line at $x=1000$ μm.

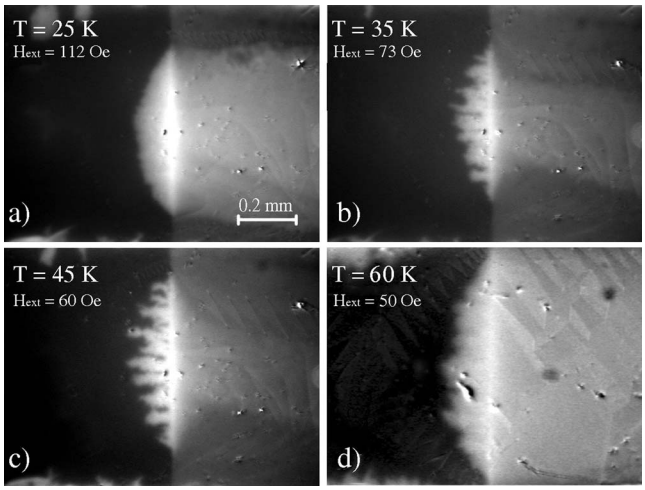

FIG. 3. Magneto-optical images taken when flux front reached a distance of 150 μm after crossing the border at (a) 25 K, (b) 35 K, (c) 45 K, and (d) 60 K. Field ramping rate for all temperatures was 0.75 Oe/s. All images were independently contrast enhanced for comfortable visualization.

at 44 K for various ramping rates. The figure clearly shows that each part of the sample is characterized by an approximately constant velocity dx/dt, exhibiting a transition from high to lower velocity at the border. The lower velocity in the irradiated part is due to the larger persistent current J which gives rise to lower magnetic diffusivity. When the ramping rate is increased from 0.1 to 1000 Oe/s, the ratio between the two velocities changes from 40 to 4, indicating that for higher ramping rates, the barrier between the two regions becomes less significant. This ratio measured for other temperatures showed similar behavior, although for lower temperatures the velocity ratio showed a milder decrease in increasing ramping rate (for example, at $T=24$ K, the ratio decreases from 5.4 to 2 as the ramping rate increases from 0.1 Oe/s to 100 Oe/s).

Measuring these velocities at a constant ramping rate with increasing temperature reveals that temperature cannot wipe out the flux diffusivity barrier even at high temperatures. As shown in Fig. 2(b), the velocity, dx/dt, measured deep in the irradiated region shows a negligible dependence on temperature, and even at 55 K, a significant difference between the velocities in the nonirradiated and the irradiated parts of the sample still exists. The figure shows that between 25 and 55 K the velocity is constant, around 4 μm/s, for a field ramp rate of 0.75 Oe/s, reflecting the weak temperature dependence of the persistent current J in the irradiated part.

Figure 3 demonstrates the creation of the finger flux patterns as the flux front crosses the border between the nonirradiated and irradiated parts of the sample. The magneto-optical images shown in the figure for the indicated temperatures depict the flux front in the irradiated part when it reaches a distance of 150 μm from the border for field ramping rate of 0.75 Oe/s. It is seen that while at 25 K [Fig. 3(a)], the front remains uniform after crossing the border (the curvature is a result of the sample geometry), at 35 K [Fig. 3(b)], the front exhibits a fingered pattern. This pattern is further enhanced at 45 K [Fig. 3(c)]. Above 50 K, the pattern gradually weakens and the front becomes smoother around 60 K [Fig. 3(d)]. These results indicate that the finger patterns appear only in an intermediate temperature range. This range also depends on the field ramp rate. At slower rates, e.g., 0.1 Oe/s, the temperature range at which fingers are observed is pushed downward, and they appear (though faintly) even below 25 K. At higher rates, i.e., 100 Oe/s and above, fingers appear at a narrower temperature range around 44 K. We note that the field range in which fingers have been observed is of the order of tens of Gauss corresponding to the irradiation matching field (40 G). Obviously, at higher fields, the columnar defects become less effective and the barrier between the two parts of the sample becomes less significant, as demonstrated in Figs. 1(b) and 1(c). We also note that although the fine details of the finger patterns are random, the place of nucleation of the fingers is reproducible.

The magneto-optical technique allows tracing the behavior of the flux front as it hits the border between the nonirradiated and irradiated parts of the sample. In Fig. 4, we show the dynamics of the flux front at 30 K for $dH_{ext}/dt = 0.75$ Oe/s. Figures 4(a)–4(e) are differential images of the time evolution of the front extracted by subtracting two consecutive images taken at a rate of 1 frame/s. The geometry of the sample that allows easy flux penetration into the nonirradiated part from only three edges creates a spearheadlike front, as shown in Fig. 4(a). Upon hitting the border, the front spreads sideways [Fig. 4(b)] along the irradiation border, and at the same time penetrates the irradiated (left hand) side with a smaller velocity, forming the fingered front shown in Fig. 4(c). Figures 4(d) and 4(e) illustrate the evolution of the fingered front as it penetrates deeper into the irradiated part, laterally spreading because of the flux motion along the border. Figure 4(f) illustrates the flux location along the border and inside the pinning enhanced region. As expected, the initial velocity along the border is higher than the velocity of the penetration through the border.

IV. DISCUSSION

Our data show that the flux diffusivity barrier, created at the border between the nonirradiated and irradiated parts of the sample, plays a central role in forming the flux finger patterns. These patterns are formed as flux crosses this border, and the fingers are always perpendicular to the border. Under experimental conditions where the barrier disappears, the finger patterns also disappear, and the flux front remains smooth upon crossing the border. Note, however, that the pattern may be smooth even in the presence of the barrier, as demonstrated at 25 K [Fig. 3(a)]. Thus, the presence of a barrier is a necessary but not sufficient condition for forming flux finger patterns. As opposed to natural edges in a bulk material, this artificial border is relatively smooth, creating favorable conditions for instabilities.[19]

The ratio of the persistent currents in the irradiated and nonirradiated parts of the sample can serve as a measure for the effective height of the barrier. This ratio can be controlled by the external field, its ramping rate, and temperature. By

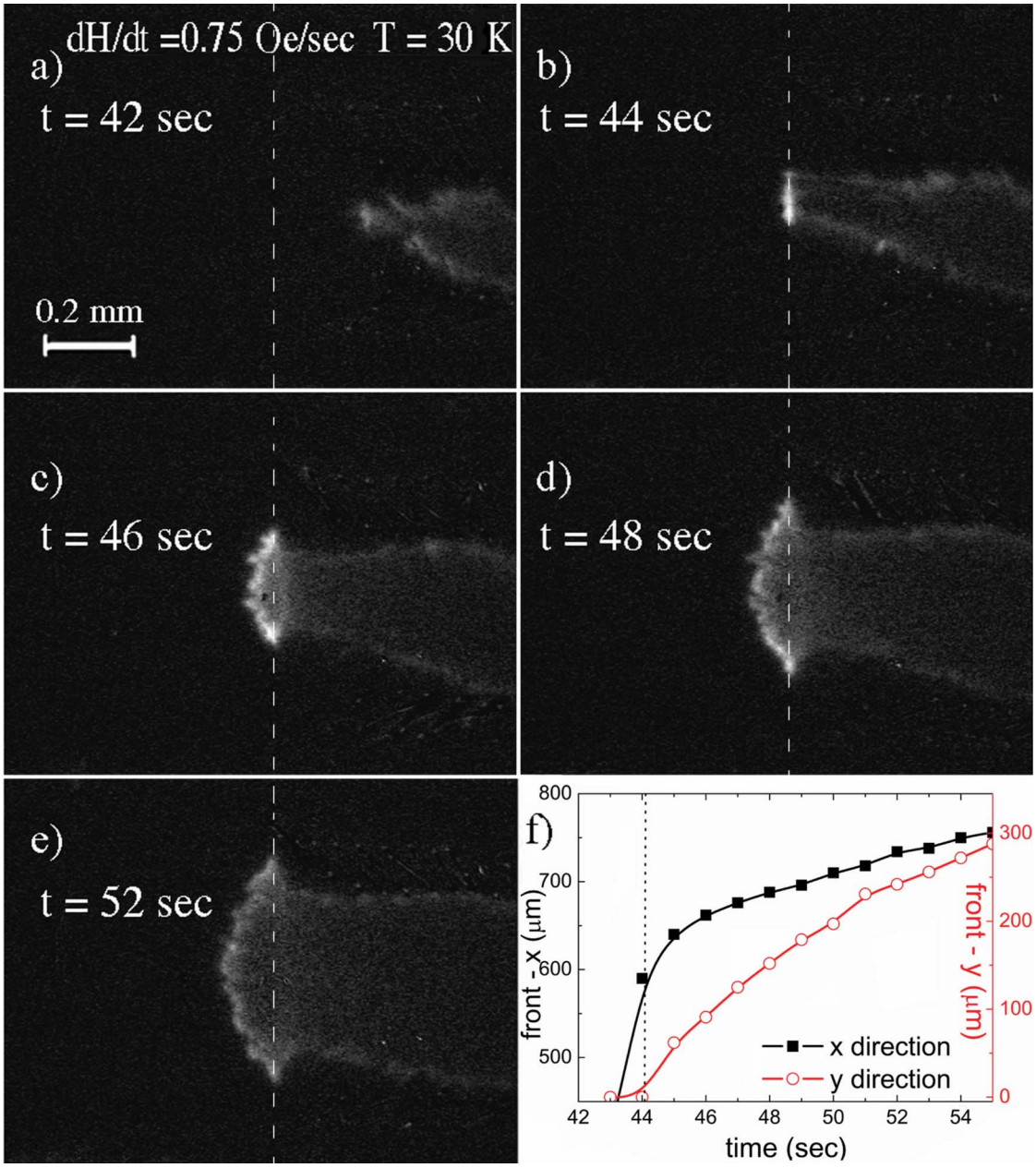

FIG. 4. (Color online) Differential magneto-optical images at 30 K, extracted by subtracting consecutive images acquired at a rate of 1 frame/s at t= (a) 42 s, (b) 44 s, (c) 46 s, (d) 48 s, and (e) 52 s. The dotted lines in (a)–(e) indicate the location of the border. Field ramping rate was 0.75 Oe/s. The front location vs time is shown in (f). (■) and (○) describe location of front through and along the border, respectively. Vertical dotted line marks time when flux collides with border.

increasing the external field, the vortex phase in the nonirradiated part of the sample can transform to a disordered phase, characterized by high persistent current density J, thus leading to reduction, or even removal of the barrier, as demonstrated in Fig. 1(b). Also, high ramping rates induce large currents in both parts of the sample, reducing the effective pinning in the irradiated part; at high enough ramping rates, the pinning in both parts of the sample becomes indistinguishable. This is demonstrated in Fig. 2(a) which shows that the front velocity $v=(dH_{ext}/dt)/J$, in the irradiated part approaches that in the nonirradiated part as the ramping rate increases. At these high rates, no fingers are observed.

The finger patterns observed in our experiments exhibit the salient features observed in films[1–7,14] and are theoretically predicted.[19–21] Namely, the fingers are perpendicular to the electric field created at the border and form a quasiperiodic structure. This suggests that the patterns observed here and in films have the same origin. However, there are several differences between our results and those reported for films. In particular, the range of existence of finger patterns is qualitatively different from that predicted and observed in films:[8,9,21,23] In our experiments, instead of the threshold magnetic and electrical fields reported for films,[8,9] we observe upper limits to these fields above which the finger pat-

terns disappear. While the apparent absence of threshold fields remains to be explored, the upper limits of those fields can be directly related to the nature of the artificial barrier produced at the border between the irradiated and nonirradiated parts of the sample. As demonstrated above, this barrier disappears at large magnetic fields and at large electrical fields (corresponding to large ramping rates of the magnetic field), thus allowing flux penetration with a smooth front.

In summary, we created an artificial barrier inside a bulk superconductor that separates regions of different magnetic diffusivity. This barrier can be controlled by changing temperature, external magnetic field, and its ramping rate. The magneto-optical technique allows direct imaging of the vortex dynamics as the flux front hits the barrier. In particular, we observed the formation of finger patterns in a wide range of temperatures and fields. The salient features of the observed patterns are consistent with the theoretical predictions suggesting that the effect is associated with thermomagnetic instabilities. A detailed theoretical treatment of the observed patterns should take into account the uniqueness of the artificial barrier and the influence of external parameters such as temperature, field, and field ramping rate on it.

ACKNOWLEDGMENTS

This research was supported in part by the Heinrich Hertz Minerva Center for High Temperature Superconductivity and the Israel Science Foundation (ISF) (Grant No. 499/07). The authors are grateful to Boris Shapiro and Eli Zeldov for many illuminating discussions and comments, to Yossi Bachar for extensive help in the analysis of the magneto-optical sequences, and to Isaschar Genish for the EDS measurements. We are particularly indebted to Marcin Konczykowski, Kees van der Beek, and Yuri Myasoedov for the irradiation of the samples.

[1] P. Leiderer, J. Boneberg, P. Brull, V. Bujok, and S. Herminghaus, Phys. Rev. Lett. **71**, 2646 (1993).
[2] B. Biehler, B.-U. Runge, P. Leiderer, and R. G. Mints, Phys. Rev. B **72**, 024532 (2005).
[3] C. A. Duran, P. L. Gammel, R. E. Miller, and D. J. Bishop, Phys. Rev. B **52**, 75 (1995).
[4] R. Surdeanu, R. J. Wijngaarden, B. Dam, J. Rector, R. Griessen, C. Rossel, Z. F. Ren, and J. H. Wang, Phys. Rev. B **58**, 12467 (1998).
[5] T. H. Johansen, M. Baziljevich, D. V. Shantsev, P. E. Goa, Y. M. Galperin, W. N. Kang, H. J. Kim, E. M. Choi, M.-S. Kim, and S. I. Lee, Supercond. Sci. Technol. **14**, 726 (2001).
[6] A. V. Bobyl, D. V. Shantsev, T. H. Johansen, W. N. Kang, H. J. Kim, E. M. Choi, and S. I. Lee, Appl. Phys. Lett. **80**, 4588 (2002).
[7] E. Altshuler, T. H. Johansen, Y. Paltiel, P. Jin, K. E. Bassler, O. Ramos, Q. Y. Chen, G. F. Reiter, E. Zeldov, and C. W. Chu, Phys. Rev. B **70**, 140505(R) (2004).
[8] F. L. Barkov, D. V. Shantsev, T. H. Johansen, P. E. Goa, W. N. Kang, H. J. Kim, E. M. Choi, and S. I. Lee, Phys. Rev. B **67**, 064513 (2003).
[9] D. V. Denisov, D. V. Shantsev, Y. M. Galperin, E.-M. Choi, H.-S. Lee, S.-I. Lee, A. V. Bobyl, P. E. Goa, A. A. F. Olsen, and T. H. Johansen, Phys. Rev. Lett. **97**, 077002 (2006).
[10] R. Prozorov, D. V. Shantsev, and R. G. Mints, Phys. Rev. B **74**, 220511(R) (2006).
[11] J. Albrecht, A. T. Matveev, J. Strempfer, H.-U. Habermeier, D. V. Shantsev, Y. M. Galperin, and T. H. Johansen, Phys. Rev. Lett. **98**, 117001 (2007).
[12] F. Colauto, E. M. Choi, J. Y. Lee, S. I. Lee, V. V. Yurchenko, T. H. Johansen, and W. A. Ortiz, Supercond. Sci. Technol. **20**, 48 (2007).
[13] J. I. Vestgaarden, D. V. Shantsev, Y. M. Galperin, and T. H. Johansen, arXiv:0709.4346v1 (unpublished).
[14] For a review, see E. Altshuler and T. H. Johansen, Rev. Mod. Phys. **76**, 471 (2004).
[15] A. V. Gurevich, Phys. Rev. Lett. **65**, 3197 (1990).
[16] A. V. Gurevich, Phys. Rev. B **46**, 3638 (1992).
[17] F. Bass, B. Y. Shapiro, and M. Shvartser, Phys. Rev. Lett. **80**, 2441 (1998).
[18] L. M. Fisher, P. E. Goa, M. Baziljevich, T. H. Johansen, A. L. Rakhmanov, and V. A. Yampol'skii, Phys. Rev. Lett. **87**, 247005 (2001).
[19] A. L. Rakhmanov, D. V. Shantsev, Y. M. Galperin, and T. H. Johansen, Phys. Rev. B **70**, 224502 (2004).
[20] I. Aranson, A. Gurevich, and V. Vinokur, Phys. Rev. Lett. **87**, 067003 (2001).
[21] I. S. Aranson, A. Gurevich, M. S. Welling, R. J. Wijngaarden, V. K. Vlasko-Vlasov, V. M. Vinokur, and U. Welp, Phys. Rev. Lett. **94**, 037002 (2005).
[22] E.-M. Choi, H.-S. Lee, H. J. Kim, B. Kang, S.-I. Lee, A. A. F. Olsen, D. V. Denisov, and T. H. Johansen, Appl. Phys. Lett. **87**, 152501 (2005).
[23] D. V. Denisov, A. L. Rakhmanov, D. V. Shantsev, Y. M. Galperin, and T. H. Johansen, Phys. Rev. B **73**, 014512 (2006).
[24] R. G. Mints and A. L. Rakhmanov, Rev. Mod. Phys. **53**, 551 (1981).
[25] Note that M. R. Wertheimer and J. le G. Gilchrist, J. Phys. Chem. Solids **28**, 2509 (1967), reported on fingered patterns in bulk alloy specimens of niobium and vanadium.
[26] N. Motohira, K. Kuwahara, T. Hasegawa, K. Kishio, and K. Kitazawa, J. Ceram. Soc. Jpn. **97**, 1009 (1989).
[27] D. Giller, A. Shaulov, T. Tamegai, and Y. Yeshurun, Phys. Rev. Lett. **84**, 3698 (2000).
[28] D. Giller, B. Kalisky, A. Shaulov, T. Tamegai, and Y. Yeshurun, J. Appl. Phys. **89**, 7481 (2001).
[29] Distortion of the dome shape is a consequence of flux penetration into the nonirradiated part from three edges only.
[30] B. Khaykovich, E. Zeldov, D. Majer, T. W. Li, P. H. Kes, and M. Konczykowski, Phys. Rev. Lett. **76**, 2555 (1996).
[31] B. Kalisky, Y. Bruckental, A. Shaulov, and Y. Yeshurun, Phys. Rev. B **68**, 224515 (2003).
[32] The two peaks observed deep inside the irradiated region, as well as the difference in induction values at the sample's edges, are due to sample imperfections.